[1]Haoyu Liu
[1*]Zhibo Yang
[2]Hongdan Zhao
[2]Keyu Yue

Analysis of Lightning Transient Characteristics of Gravity Grounding Devices for Offshore Wind Turbines

Journal of Electrical Systems

Abstract: When lightning current strikes the blade lightning arrester and travels through the down conductor and tower, it forms a wave process that impacts the impulse grounding resistance and ground potential rise of the grounding device. To study the transient characteristics of gravity grounding devices for offshore wind turbines under lightning strikes, a novel comprehensive model of offshore wind turbines was developed. This model integrates the Method of Moments (MoM) and Fourier transform, considering the complete path of lightning current from the wind turbine to the ground. The model includes blades, tower, and grounding device. The study examines the effects of varying seawater depths, silt layer soil resistivities, lightning current waveforms, and tower heights on the impulse characteristics of grounding devices during lightning strikes on wind turbine blades. The influence mechanism is analyzed using wave process theory. Calculations indicate that when the seawater depth is 0 m, the impulse grounding resistance significantly increases with the rise in soil resistivity of the silt layer. As the seawater depth increases, the influence of silt layer soil resistivity on impulse grounding resistance diminishes significantly. The shorter the lightning current wavefront time, the higher the potential rise of the grounding device. However, when the wavefront time of the lightning current is long, the oscillation attenuation of the grounding device's potential rise is not significant. The height of the wind turbine tower affects the oscillation frequency of the ground potential rise of the grounding device, with the oscillation frequency being inversely proportional to the tower height.

Keywords: Grounding device; Impulse characteristics; Lightning transient process; Method of Moments; Offshore wind turbines.

I. Introduction

With the continuous advancement of new energy technologies, offshore wind power has become one of the hotspots in the global new energy sector [1-2]. Currently, in the context of vigorously developing offshore wind energy, the operating environment of wind turbines is becoming increasingly harsh, characterized by humid and rainy maritime atmospheres and frequent thunderstorms. Additionally, the continuous increase in the individual capacity of wind turbines and the overall height of the turbines significantly enhance their lightning-triggering capability, thereby increasing the likelihood of lightning strikes on wind turbines [3]. During the transient process of lightning current discharging from the top to the bottom of the entire wind turbine, a transient strong electromagnetic field is generated inside the wind turbine tower. This can interfere with power lines, signal devices, monitoring, and control systems, thereby threatening the safe and stable operation of the wind turbine. Furthermore, the transient potential at various parts of the wind turbine can change due to the action of lightning current, causing potential rise phenomena that may result in equipment malfunctions or insulation damage, potentially leading to severe consequences such as personal injury. Therefore, the characteristics of the wind turbine grounding system are crucial factors in the study of lightning electromagnetic effects and lightning protection for wind turbines.

Currently, numerous studies have been conducted on the grounding characteristics of onshore wind turbines [4-11], but research on the grounding characteristics of offshore wind turbines is relatively scarce [12]. Due to the unique nature of the marine environment, the rules applicable to onshore wind farms cannot be simply applied to the grounding design of offshore wind farms [13-15]. In terms of operating environment, the differences between offshore and onshore wind farms are significant. Most offshore wind turbine foundations are located below sea level most of the time, and seawater has a very strong dispersing capacity. Therefore, most offshore wind turbines use their natural foundations as natural grounding electrodes.

In China, the construction and planning of offshore wind farms show a certain preference for intertidal zones. The coastal areas of Jiangsu, Shanghai, and Shandong are concentrated areas for intertidal zone resources, particularly north of the Yangtze River estuary, where the concentration of intertidal zone resources is high. Intertidal zone wind power generation, with its advantages of being closer to power load centers and lower development costs,

[1] School of Electrical Engineering, Northeast Electric Power University, Jilin 132012, Jilin, China

[2] State Grid Jilin Electric Power Co., Ltd., Liaoyuan Power Supply Company, Liaoyuan 136200, Jilin, China

[*]Email: 2202100270@neepu.edu.cn

[*]Corresponding author

aligns with the basic national conditions of China [16]. Gravity grounding devices are generally used in offshore intertidal zones, and gravity-based offshore wind turbine foundations have been successfully applied in the intertidal wind farm in Rudong, Jiangsu, China [17].

The lightning impact characteristics of grounding devices are crucial for grounding scheme design and are also one of the key research focuses in wind turbine lightning protection. Reference [4] studied the effects of wind turbine blades and towers on the grounding system and transient characteristics of tower lightning strikes. Due to the large total height of the blades and towers, lightning currents can form wave processes within them. At this point, the current entering the ground differs significantly from the injected lightning current, which affects the actual ground potential rise. Reference [18] used the method of moments to analyze the lightning overvoltage at the bottom of wind turbine towers. The results showed that considering the steel bars in concrete can significantly reduce the lightning impact grounding resistance of wind turbines and the potential rise at the bottom of the tower, with a more pronounced effect in areas with high soil resistivity. The study also discussed the influence of the number and distribution of vertical piles in wind turbine foundations on the lightning impact grounding resistance and potential rise at the bottom of the tower. Reference [19] systematically calculated the frequency domain characteristic parameters and impact characteristic parameters of gravity foundations using CDEGS simulation software, discussing the effects of various conditions on the frequency domain grounding resistance and lightning impact grounding resistance, and summarizing their laws. Reference [20] conducted a simulation study on offshore wind turbines using high-pile pedestal foundations as natural grounding electrodes, considering tidal fluctuations and pedestal resistivity, and calculating the frequency domain grounding resistance and lightning impact grounding resistance. The above references provide detailed introductions to the research on wind turbine grounding devices, but there is little introduction to the overall model including wind turbine blades, towers, and grounding devices, making it difficult to consider wave processes and their analysis of lightning transient characteristics on grounding devices.

Based on the frequency domain moment method, the author establishes an equivalent model of wind turbine lightning electromagnetic transients including wind turbine blades, towers, and grounding devices. The time-domain responses of the ground potential rise and current of the wind turbine grounding device are obtained using the moment method and Fourier transform. The lightning transient characteristics of the wind turbine grounding system are analyzed computationally. Considering that gravity-based foundations are generally used in coastal tidal zones, tidal fluctuations and actual soil environments are taken into account. The influence of seawater depth, silt layer resistivity, tower height, and lightning current waveform on the lightning impact characteristics of wind turbine grounding devices is discussed.

II. Computational Model

When lightning strikes the lightning arrester on wind turbine blades, the lightning current is conducted through the down conductor in the blades to the wind turbine tower and then transmitted to the ground through the grounding device. Based on the frequency domain moment method, a computational analysis model has been established, which includes three parts: the down conductor in the blades, the tower, and the grounding system.

The length of the down conductor in the wind turbine blades is approximately 50 meters. The height of the tower is approximately 50-100 meters, with a top outer diameter of 2.5 meters and a bottom outer diameter of 4.2 meters. The schematic diagram of the steel structure of the gravity-based foundation is shown in Fig. 1. The outer diameter of the gravity-based foundation is 12 meters, with a height of 3 meters, and the inner diameter is 5 meters, with a height of 12 meters. Six partitions are uniformly installed between the inner and outer walls, each partition being 4 meters high.

The gravity-based foundation in this study adopts a prefabricated circular cavity structure filled with concrete, enabling it to withstand external loads such as the total weight of the wind turbine and tower, wind loads, and seismic loads, and to remain stable under adverse sea conditions, preventing slipping and overturning. The concrete covers the foundation steel structure, forming many tiny air holes inside. Due to the characteristics of concrete, the air holes in the concrete can absorb the pore liquid in the surrounding soil when the concrete contacts the moist soil. Therefore, groundwater and moisture content need to be considered, and the electrical conductivity of concrete is related to the characteristics of the surrounding soil. Currently, in grounding device construction, the grounding resistance of concrete is generally considered equivalent to the surrounding soil. In grounding calculations, concrete is usually treated as equivalent to the surrounding soil. When establishing grounding device models, such as in references [11, 19], concrete is regarded as the surrounding soil, and the difference between concrete in pile foundations and the surrounding soil is ignored. When analyzing the grounding impedance characteristics of wind turbines, as in references [22-23], the difference between concrete in pile foundations and the surrounding soil is also ignored, resulting in theoretical calculation values that are close to the measured results. Similar treatment methods are also adopted in reference [24]. In this study, the gravity-based foundation is located on the seabed, and concrete is treated

as equivalent to the surrounding soil in the model.

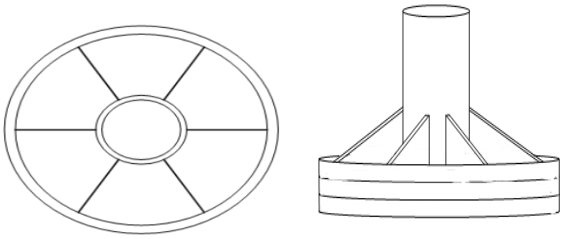

Fig. 1. Top and front view of the grounding device

The tower base, serving as the natural grounding body for offshore wind turbines, needs to be modeled according to actual conditions, taking into account terrain characteristics and external environmental factors. The intertidal zone refers to the coastline between the average high tide and low tide levels. Due to the ebb and flow of tides, the depth of seawater varies between 0 and 10 meters, and there is a large amount of sediment in the intertidal zone. Therefore, soil is considered in three layers, namely the seawater layer, the sludge layer, and the sand and gravel layer, as shown in Fig. 2.

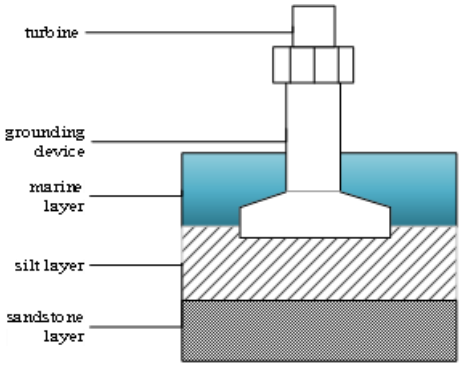

Fig. 2. Soil model

The seawater layer has a depth of 0-10m with a resistivity of 1Ω·m, the sludge layer is 10m thick with a burial depth of 2m and a resistivity ranging from 60 to 1500Ω·m, and the sand and gravel layer has a resistivity of 1000Ω·m.

In this study, a slender wire model is adopted [4], where metal conductors are represented by slender conductors. Due to the difficulty of using the moment method to analyze cylindrical structural models, multiple slender conductors are used to equivalent metal surfaces. When modeling the wind turbine, it is necessary to consider the shape and position of the blades, tower, and grounding device.

The down conductor of the blade is equivalent to a single slender conductor; the tower is represented by 12 slender conductors to construct a hollow frustum structure for equivalence; the grounding foundation base is equivalent to 24 slender conductors each with a length of 6m; the outer wall of the base is represented by 72 slender conductors; the inner wall is simulated by 12 slender conductors; 6 symmetrical partitions are placed between the outer and inner walls, each partition being simulated by 8 slender conductors. The overall model of the wind turbine is shown in Fig. 3.

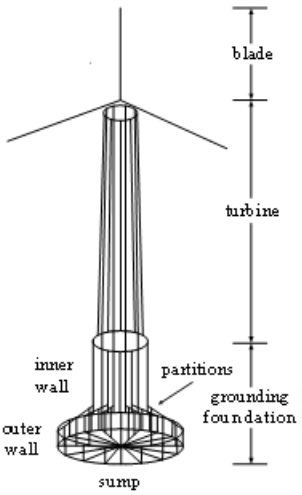

Fig. 3. Wind turbine overall model diagram

When calculating the electromagnetic field distribution, the distribution of current across the conductor cross-section is not considered, and the current is assumed to be concentrated at the center of the conductor, as shown in Fig. 4(a). The axial current of the conductor is taken as a variable, and the current model of the triangular function is used as the current basis function. At the surface of each straight conductor segment, the electric field intensity inside and outside the conductor should satisfy the boundary conditions in Equation (1).

$$n\times(E^i+E^s)=0 \qquad (1)$$

where n is the normal direction outside the surface of the cylindrical conductor; E^i is the external electric field intensity applied to the surface of the conductor; E^s is the internal electric field intensity generated by the axial current of the conductor itself.

$$E^s=-j\omega A-\nabla\varphi \qquad (2)$$

where A represents the electromagnetic vector potential generated by the axial current; φ represents the electromagnetic scalar potential; Ω represents the angular frequency.

$$A=\frac{\mu}{4\pi}e\times\int_{l'}I(l)\frac{e^{-jkr}}{r}dl \qquad (3)$$

$$\varphi=\frac{1}{4\pi\varepsilon}\int_{l'}\nabla I(l)\frac{e^{-jkr}}{r}dl \qquad (4)$$

where e represents the axial direction of the line current in the cylindrical conductor; r represents the distance vector between the source point and any observation point on the surface of the conductor, in units of m; μ, ε respectively represent the magnetic permeability and dielectric constant of the space where the conductor is located; k represents the wave vector, in units of rad/m,

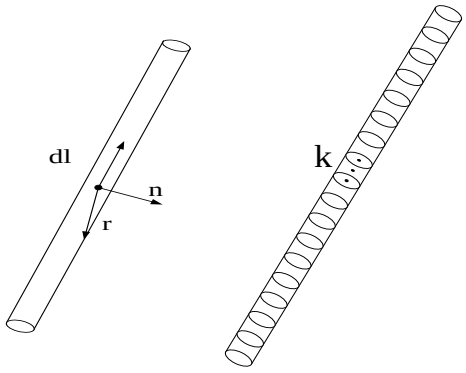

(a) Any thin wire (b) Division of wires

Fig. 4. Schematic diagram of thin wire

Furthermore, the external electric field strength E^s at the midpoint of the conductor segment is equal to the potential difference U_K per unit length along the axial current, hence:

$$E^s=Z_c^kI(l)=U_k \qquad (5)$$

Assuming the entire conductor structure is segmented into N segments, as shown in Fig. 4(b), the following system of linear algebraic equations can be obtained:

$$U_k=\sum_{i=1}^{N}Z_{ik}I_i \qquad k=1,2,\cdots,N \qquad (6)$$

Where Z_{ik} is the mutual impedance between the ith and kth conductor segments (when $i\neq k$), or the self-impedance of the kth segment (when $i=k$); the matrix form of Equation (6) is given by:

$$ZI=U \qquad (7)$$

The current distribution on each conductor segment is approximated by trigonometric functions, and the current is expressed as:

$$I(l)=A+B\sin kl+C\cos kl \qquad (8)$$

Where A, B, and C are undetermined coefficients.

At the junctions of conductors with different radii or at the intersections of multiple conductors, the linear

charge density satisfies the relationship given in Equation (9).

$$\frac{\partial I(l)}{\partial l} = \frac{Q}{In(\frac{2}{ka}) - \gamma} \quad (9)$$

Where, a is the radius of the conductor, and Euler's constant, γ is 0.5772. Q is a value related to the total charge in the region of the conductor intersection point and is the same for all conductors connected to this point. The end effects of the conductors are neglected, and the current and charge at the endpoints of floating conductors, where no current is injected, are assumed to be zero. By applying the continuity equations for both current and charge at the intersection points, the total number of unknowns is equal to the number of conductor segments.

The external excitation source for the wind turbine adopts a current source, meaning the current at one end of the conductor is a known quantity. Using equation (7), other unknown currents can be determined. Following the above calculation process, the current distribution on each conductor segment at a specific frequency can be obtained, thereby calculating the electric field strength at that frequency.

By combining the above calculation process with the fast Fourier transform, the lightning current waveform undergoes Fourier transformation to determine the calculation frequency. The frequency domain response is then calculated using the method of moments, and the time domain response is obtained using the inverse Fourier transform. This allows for the calculation of the transient current and potential rise on the wind turbine grounding system when struck by lightning, subsequently computing the impulse grounding resistance. The principle of the wind turbine lightning transient process calculation is shown in Fig. 5.

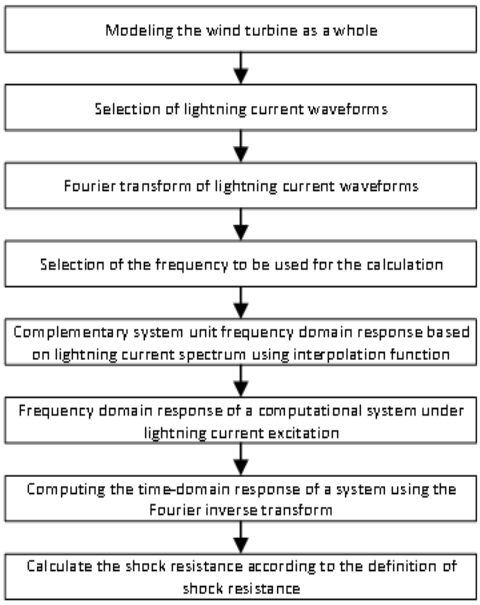

Fig. 5. Schematic diagram of the transient process of a wind turbine

III. Influence of Seawater Depth

Due to the use of natural grounding bodies as the foundation, the dispersion of lightning current primarily occurs in the seawater layer. Therefore, the grounding characteristics of offshore wind turbines will vary with the tides in the actual operation of offshore wind farms.

Considering a tower height of 80 meters and a silt layer resistivity of 60 Ω·m, with a 2.6/50 μs lightning current waveform as the excitation source and a lightning current amplitude of 100 kA, the potential rise of the wind turbine grounding system when the lightning strikes the tip of the turbine blade was calculated, as shown in Fig. 6 and Fig. 7. It can be seen that the transient potential rise waveform in the wind turbine grounding system exhibits a significant oscillation process, which gradually attenuates over time. The wave process theory is used below to analyze the aforementioned process.

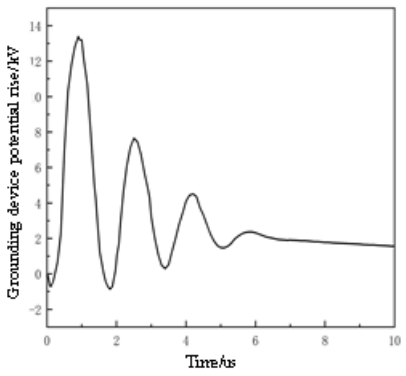

Fig. 6. The grounding device potential rises (0m in seawater layer)

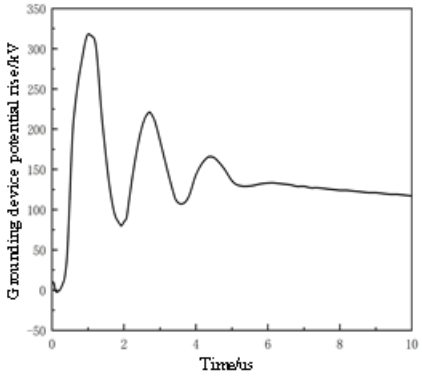

Fig. 7. The grounding device potential rises (0m in seawater layer)

The down conductor of the wind turbine blade and the tower can be equivalently viewed as a transmission line with a wave impedance Z while the grounding system is represented as a lumped parameter impedance Z_L .Typically, there is a significant difference between the values of Z and Z_L, resulting in a refraction and reflection process at their junction. The total height of the down conductor and the tower is h, and the propagation speed of the lightning current wave I along the tower is v=300 m/μs.When the lightning current wave I reaches the junction of the tower and the grounding device, a reflection and refraction phenomenon occurs. Part of the lightning current wave flows into the seawater and the ground through the grounding system, while the other part reflects back up the tower. Assuming the reflection coefficient is $\beta(\beta=(Z_L-Z)/(Z_L+Z))$, the current wave β_1 fully reflects when it reaches the tip of the blade, with a reflection coefficient of 1. Considering that $Z>Z_L$ under normal conditions, β is negative. Therefore, the first reflected current wave reaches the base of the tower at $t=3h/v$ with an amplitude of $\beta_1 I$. Since $\beta_1<0$, the first reflected current wave ($\beta_1 I$) reduces the current flowing into the grounding device, thereby attenuating the ground potential rise oscillation generated by the grounding device. The second reflected current wave reaches the base of the tower at $t=5h/v$, when the second reflected current wave ($\beta_2 I$) increases the current flowing into the grounding device, enhancing the ground potential rise. This process continues accordingly, so when $t=(2k+1)h/v$, the current wave I_j on the grounding device is:

$$I_j = \alpha(1+\beta_1+\beta_2+\cdots+\beta_k)I \quad (10)$$

When k is an odd-numbered term, $\beta_k I$ is negative, primarily serving to weaken the ground potential rise. When k is an even-numbered term, $\beta_k I$ is positive, primarily enhancing the ground potential rise. The ground potential rise on the grounding device is repeatedly weakened or enhanced as the current reflection wave propagates. Therefore, the current wave on the wind turbine tower oscillates with a period of $4h/v$ or an oscillation frequency of $v/4h$ Generally, the absolute value of $\beta_k I$ decreases as the reflection count k increases, resulting in a noticeable oscillatory decay trend in the transient lightning current waveform on the grounding system. Moreover, the absolute value of the odd-numbered terms; $\beta_k I$ is larger than the corresponding even-numbered terms, i.e., $\alpha(\beta_{2k-1}+\beta_{2k})I<0$($\alpha$ is the refraction coefficient, $\alpha=2Z_L/(Z_L+Z)$), causing each oscillation cycle to decrease the potential rise on the grounding device.

Comparing the results from Fig. 6 and Fig. 7, it can be observed that the amplitude of the ground potential rise on the grounding device decreases as the depth of seawater increases, but the oscillatory phenomenon remains pronounced. This is because with greater seawater depth, the grounding device experiences more significant dissipation effects, resulting in a lower grounding resistance value and thus a reduced amplitude of the ground potential rise. According to the theory of wave reflection and refraction, the oscillation becomes more pronounced under these circumstances.

Fig. 8 illustrates the variation of the wind turbine grounding system's impulse ground resistance with seawater depth. It can be seen from Fig. 8 that the impulse ground resistance rapidly decreases as the seawater depth increases from 0 meters to 1 meter. As the seawater depth continues to increase, the impulse ground resistance gradually decreases, with a very slow reduction rate beyond 5 meters, ultimately reaching a stable state.

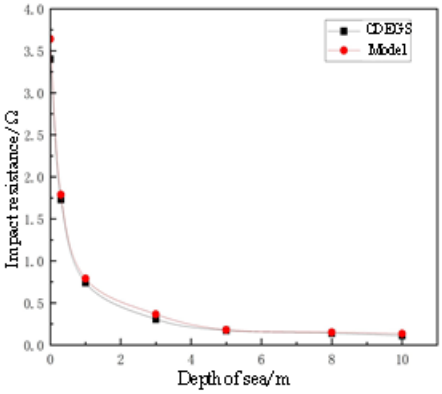

Fig. 8. Effect of seawater depth on impulse resistance

From Fig. 8, it can be observed that the impulse ground resistance calculated from the wind turbine's overall model shows minimal deviation from the results obtained using CDEGS in reference [18]. Moreover, both sets of results exhibit consistent variation patterns, demonstrating the accuracy of the model proposed in this study.

IV. Impact of Mud Layer Soil Resistivity

The resistivity of the mud layer soil affects the transient characteristics of the grounding device by influencing its equivalent aggregate parameter impedance, thereby affecting the transient process. Therefore, when studying the influence of mud layer soil resistivity on the impulse characteristics of the grounding device, only the impulse resistance is calculated. Taking a turbine tower height of 80m and a lightning current waveform of 2.6/50μs as examples, the ground potential rise and lightning current waveform are obtained when the lightning current strikes the wind turbine blade tip discharge device. Different scenarios of impulse ground resistance are defined based on the impulse resistance, as depicted in Fig. 9 and Fig. 10.

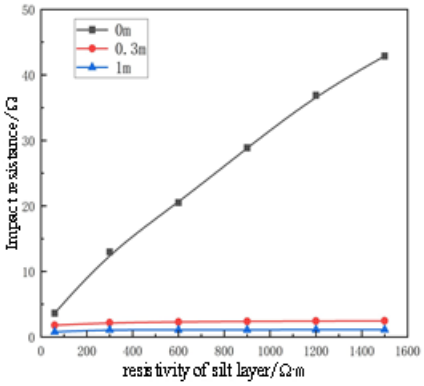

Fig. 9. Effect of Resistivity of Silt Layer on Impulse Resistance at Different Seawater Depths (0-1m in Seawater Layer)

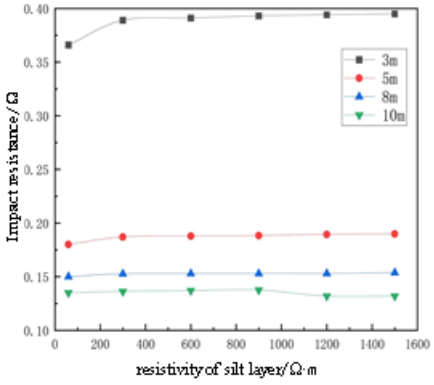

Fig. 10. Effect of Resistivity of Silt Layer on Impulse Resistance at Different Seawater Depths (3-10m in Seawater Layer)

Combining Fig. 9 and Fig. 10, it can be observed that the impulse ground resistance increases with the increase in mud layer soil resistivity. However, the influence of mud layer soil resistivity on the impulse ground resistance gradually diminishes with the increase in seawater depth. When the seawater depth is 0 meters, indicating no seawater intrusion into the grounding device, the impulse ground resistance significantly increases as the mud layer soil resistivity increases (from 60Ω·m to 1500Ω·m), resulting in a notable increase in impulse ground resistance (from 3.64Ω to 42.89Ω). As the seawater depth gradually increases from 0.3m to 10m, the extent of the influence of mud layer soil resistivity on the impulse ground resistance decreases. When the seawater depth reaches 10m, with the mud layer soil resistivity increasing from 60Ω·m to 1500Ω·m, the impulse ground resistance only increases from 0.135Ω to 0.139Ω. The variation in impulse ground resistance with mud layer soil resistivity can be considered negligible at a seawater depth of 10m.

V. Impact of Lightning Current Waveform

The transient characteristics of the wind turbine grounding system are not only influenced by the seawater depth and mud layer resistivity but also by the waveform parameters of the lightning current. Below is a comparative analysis of the transient ground potential rise of the wind turbine grounding system under different waveform parameters of the lightning current excitation. Taking a tower height of 80m, blade length of 50m, mud layer soil resistivity of 60Ω·m, and seawater depths of 10m and 0m, the transient ground potential rise of the wind turbine grounding system is calculated under standard lightning current excitations with amplitudes of 100kA and waveforms of 1.2/50μs, 2.6/50μs, and 8/20μs, respectively. The results are shown in Fig. 11 and Fig. 12.

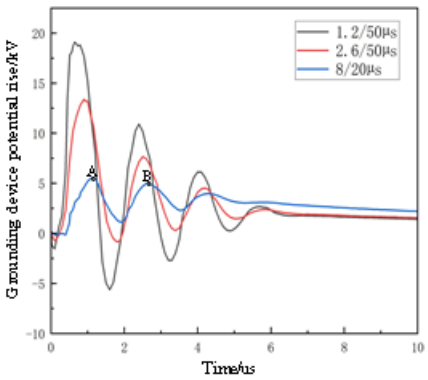

Fig. 11. Grounding potential rise under different lightning current waveforms (10m in seawater layer)

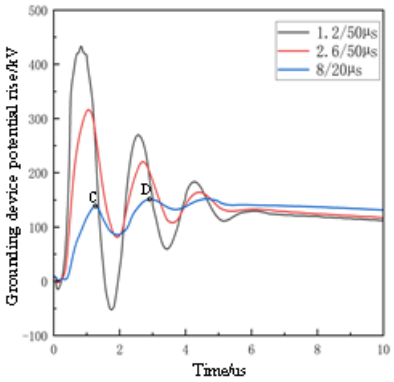

Fig. 12. Grounding potential rise under different lightning current waveforms (0m in seawater layer)

When the seawater depth is 10m (as shown in Fig. 11), the maximum ground potential rise amplitude of the 1.2/50μs waveform (19.10 kV) is approximately four times that of the 8/20μs waveform (5.48 kV). When the seawater depth is 0m (as shown in Fig. 12), the maximum ground potential rise amplitude of the 1.2/50μs waveform (434.81 kV) is approximately 300 kV higher than that of the 8/20μs waveform (151.79 kV). The ground potential rise amplitudes of the wind turbine grounding system show significant differentiation due to the high impedance characteristics of the grounding system. When the front time of the lightning current waveform decreases, there is a greater transient potential rise on the grounding system, as the transient impedance of the grounding system is higher, leading to an increase in the energy of high-frequency current components.

From Fig. 11 and Fig. 12, it can be observed that when the lightning current waveform is 8/20μs, with a seawater depth of 10m, the first peak of the ground potential rise on the grounding device is 5.48 kV (point A), and the amplitude of the second peak is 4.97 kV (point B), with little difference between them. When the seawater depth is 0 m, the first peak of the ground potential rise on the grounding device is 140.26 kV (point C), and the amplitude of the second peak is 151.79 kV (point D), with the second peak of the ground potential rise on the grounding device being slightly higher than the first peak. This contradicts the general rule of low potential rise oscillation decay mentioned earlier. The analysis of the reasons is as follows:

After the lightning strikes the top of the wind turbine blades, when the lightning current i flows from the bottom of the tower to the grounding device, the ground potential rise U_e on the grounding device can be approximately represented as:

$$U_e = \mathrm{L}\frac{di}{dt} + i\mathrm{r} \qquad (11)$$

L represents the self-inductance of the grounding device conductor, while r denotes the resistance of the surrounding soil. The voltage generated as the lightning current flows through L and r superimposes on the grounding device, thereby causing the ground potential to rise. The inductance L remains relatively constant when the size and material of the grounding device remain unchanged. As the soil resistivity increases, r also increases, leading to a higher value of U_e.

When the duration of the lightning current is relatively long (8/20μs), as shown in Fig. 12, the amplitude of the first peak of the ground potential rise (140.26 kV) is lower than that of the second peak (151.79 kV). This is because the waveform time of the lightning current (8μs) is much longer than the durations of the first peak (1.25μs) and the second peak (2.95μs). During the waveform time, the lightning current, i is in a rapid growth phase, and the value of $L(di/dt)$ can be considered constant. When the seawater depth is 0m, the high resistivity of the dispersion layer (60Ω·m) leads to an increase in the value of ir resulting in the second peak of the ground potential rise (151.79kV) being higher than the first peak (140.26kV), as indicated by points C and D in Fig. 12. When the seawater depth is

10m, the low resistivity of the dispersion layer (1Ω·m, mainly seawater) results in little change in the value of Thus, the difference between the amplitudes of the first peak (5.48kV) and the second peak (4.97kV) of the ground potential rise is not significant, as shown by points *A* and *B* in Fig. 11.

VI. The Influence of Tower Height

When the wind turbine blades are struck by lightning, the process of lightning current flowing from the tower to the ground through the grounding device undergoes changes due to the presence of reflection and refraction processes at the junction between the tower and the grounding device. Consequently, this will alter the transient ground potential rise generated on the grounding device. The reflection and refraction time of lightning current at the junction between the tower and the grounding system will vary with changes in the height of the wind turbine tower, thereby causing changes in the oscillation frequency of the transient potential rise waveform in the grounding system. Using a lightning current waveform with an amplitude of 100 kA and a duration of 2.6/50μs, and assuming a soil resistivity of 60Ω·m, the transient ground potential rise of the wind turbine grounding system is calculated for tower heights of 50m, 80m, and 100m, as shown in Fig. 13 and Fig. 14.

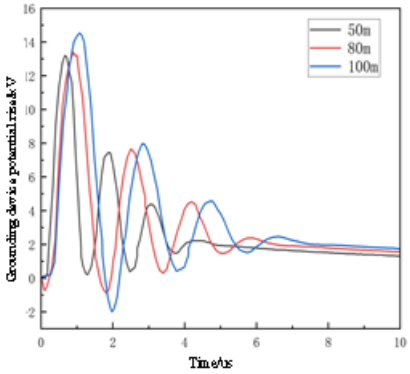

Fig. 13. Grounding potential rise at different tower heights
(10m in seawater layer)

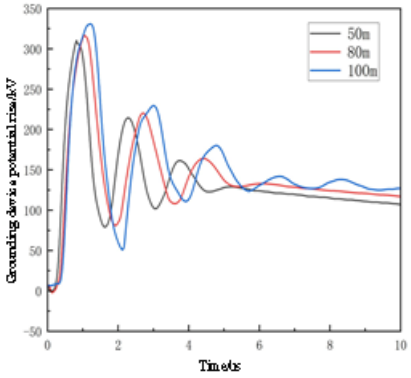

Fig. 14. Grounding potential rise at different tower heights
(0m in seawater layer)

From Fig. 13 and Fig. 14, it can be observed that the oscillation frequency of the transient ground potential rise waveform on the wind turbine grounding system varies significantly with different tower heights, while there is a minor difference in the amplitude of the ground potential rise on the grounding system. When the sea depth is 10m (Fig. 13), the oscillation frequencies for tower heights of 50m, 80m, and 100m are 0.741MHz, 0.633MHz, and 0.601MHz respectively. When the sea depth is 0m (Fig. 14), the oscillation frequencies for tower heights of 50m, 80m, and 100m are 0.698MHz, 0.591MHz, and 0.546MHz respectively. The variation in tower height leads to changes in the reflection period of lightning current waves on the tower, which is due to the principles of wave propagation theory. Different tower heights result in different reflection periods of lightning current waves on the tower, thereby causing variations in the oscillation frequency of the transient ground potential rise on the grounding system. As the tower height increases, the reflection period of the lightning current wave on the tower increases, leading to a decrease in the oscillation frequency of the ground potential rise on the grounding system. At the same time, the amplitude of the ground potential rise on the grounding system slightly increases with increasing tower height, but the effect is minimal.

VII. Conclusion

In summary, based on the frequency-domain moment method, an equivalent model of the gravity-type grounding device for offshore wind turbines has been established, and the effects of different scenarios on the transient process of the grounding device have been analyzed. The following conclusions have been drawn:

(1) The depth of seawater is the primary influencing factor on the impulse resistance of the grounding device. When the tower height is 80m, the resistivity of the mud layer is 60 Ω·m, and the excitation source adopts a 2.6/50 μs lightning current waveform, the impulse resistance decreases from 3.64 Ω to 0.18 Ω as the seawater depth increases from 0m to 5m. When the seawater depth increases from 5m to 10m, the impulse resistance decreases from 0.18 Ω to 0.13 Ω, and the decreasing trend of the impulse resistance becomes more gradual.

(2) The impedance of the equivalent aggregated parameters of the grounding device is jointly affected by the resistivity of the mud layer and the depth of seawater, thereby influencing the transient process of lightning current.

Specifically, the smaller the impulse resistance, the smaller the amplitude of the ground potential rise on the grounding device, but the more pronounced the oscillation decay.

(3) The leading edge time of the lightning current has a significant impact on the amplitude of the ground potential rise on the grounding device. The shorter the leading edge time of the lightning current, the greater the amplitude of the ground potential rise on the grounding device. However, when the leading edge time is long, the oscillation decay of the ground potential rise on the grounding device is not significant. This phenomenon is also noteworthy for lightning protection.

(4) The tower height of the wind turbine affects the oscillation frequency of the ground potential rise on the grounding device. The higher the tower, the lower the oscillation frequency of the ground potential rise on the grounding device. When the tower height increases from 50m to 100m, the oscillation frequency decreases from 0.741 MHz to 0.602 MHz.

Acknowledgments

This paper was supported by Natural Science Foundation of Jilin Province (No. 20230101340JC).

References

[1] Garolera A C, Madsen S F, Nissim M, et al. Lightning damage to wind turbine blades from wind farms in U.S [J]. IEEE Trans. on Power Delivery, 2016, 31(3): 1043-1049.

[2] Luo Dehong. Current status and countermeasures of offshore wind power development in China [J]. Hydropower and New Energy, 2022, 11(36): 76-78.

[3] Tao Jiangen, Chen Yi, Huang Boyuan. Analysis of the current status and trends in offshore wind power development [J]. Energy Engineering, 2023, 43(4): 1-9.

[4] Zhang Bo, Xue Huizhong, Zhang Baoquan, et al. The impact of blades and tower on the impulse grounding characteristics of grounding devices during wind turbine lightning strikes [J]. High Voltage Engineering, 2012, 38(10): 2675-2682.

[5] Fan Kai. Study on power frequency grounding characteristics of wind turbine grounding devices [J]. Electrical Engineering, 2023, (06): 65-67.

[6] Shi Liu, Li Liming, Xuan Ming, et al. Analysis of transient characteristics of wind turbine grounding systems under lightning impulse [J]. Heilongjiang Electric Power, 2023, 45(04): 305-309.

[7] Wan Xingyu, Zhang Zhonghui. Analysis of transient characteristics of wind turbine grounding systems under lightning strikes [J]. Electrical Insulator and Surge Arrester, 2018, (1): 64-76.

[8] Xie Xuanying, Lin Yiping, Liu Shufeng, et al. Transient analysis of wind turbine tower base lightning based on ATP-EMTP [J]. Meteorological Hydrological and Marine Instruments, 2023, 40(04): 45-48.

[9] Zhang Ping, Yang Xiaolei, Li Yongjian, et al. Virtual simulation experiment of offshore wind turbine lightning electromagnetic transients based on ANSYS [J]. Experimental Technology and Management, 2022, 39(10): 86-90.

[10] Elmghairbi A, Haddad A, Griffiths H. Potential rise and safety voltages of wind turbine earthing systems under transient conditions [C]//20th International Conference on Electricity Distribution-Part 1. Prague, Czech Republic: IET, 2009: 1-4.

[11] Yamamoto K, Yanagawa S, Yamabuki K, et al. Analytical surveys of transient and frequency-dependent grounding characteristics of a wind turbine generator system on the basis of field tests [J]. IEEE Transactions on Power Delivery, 2010, 25(4): 3035-3043.

[12] Wang Guozheng, Zhang Li, Wu Hao, Zhao Tong, Zou Liang. Integrated electromagnetic transient model and lightning transient overvoltage study of offshore wind turbines [J]. Electric Power Automation Equipment, 2017, 37(11): 32-38.

[13] Wang Licun, Wei Jing, Wang Xudong, et al. The development and prospect of offshore wind power technology in the world [C]. IEEE Power and Energy Society General Meeting -Conversion and Delivery of Electrical Energy in the 21st Century. Pittsburgh, USA: IEEE, 2008: 1-2.

[14] Ge Chuan, He Yanping, Ye Yu, et al. Development, composition, and foundation forms of offshore wind farms [J]. China Offshore Platform, 2008, 23(6): 31-35.

[15] JB/T10300-2001. Design requirements for wind turbines [S]. Beijing: National Energy Administration, 2012.

[16] Li Meiming, Xu Qunjie, Han Jie. Research and application status of corrosion protection for offshore wind power [J]. Corrosion and Protection, 2014, 35(6): 584-589, 622.

[17] Wu Zhiliang, Wang Fengwu. Types and calculation methods of offshore wind turbine foundations [J]. Waterway Engineering, 2008, (10): 249-258.

[18] Sun Tong, Li Wei, Zhang Bo, et al. Analysis of transient processes of lightning strikes at the base of wind turbine towers considering natural grounding bodies [J]. Electrical Insulator and Surge Arrester, 2022, (1): 29-35.

[19] Zhou Mi, Fan Yadong, Zheng Zhongnan, et al. Grounding characteristics of gravity-based foundations for offshore wind turbines in the intertidal zone [J]. Power Grid Technology, 2015, 39(11): 3320-3326.

[20] Li Jutian, Peng Qian, Fang Chaoying, et al. Simulation study on using high pile cap foundations as self-grounding bodies for offshore wind turbines [J]. Electrical Insulator and Surge Arrester, 2016, (5): 114-119.

[21] Shen Haibin, Kang Peng, Bian Kai, et al. Experimental study on grounding characteristics of 10kV distribution line reinforced concrete poles [J]. Power Grid Technology, 2014, 38(6): 1670-1675.

[22] Yamamoto K, Noda T, Yokoyama S, et al. Experimental and analytical studies of lightning overvoltages in wind turbine generator systems [J]. Electric Power Systems Research, 2009, 79(3): 436-442.

[23] Yamamoto K, Yanagawa S, Sekioka S, et al. Transient grounding characteristics of an actual wind turbine generator system at a low resistivity site [J]. IEEJ Transactions on Electrical and Electronic Engineering, 2010, 5(1): 21-26.

[24] Kostic M B. Analysis of complex grounding systems consisting of foundation grounding systems with external grids [J]. IEEE Transactions on Power Delivery, 1998, 13(3): 752-756.